Available online at www.sciencedirect.com
SCIENCE DIRECT®
Icarus 169 (2004) 111–126
ICARUS
www.elsevier.com/locate/icarus

Ridges and tidal stress on Io

Gwendolyn D. Bart,[a,*] Elizabeth P. Turtle,[a] Windy L. Jaeger,[a] Laszlo P. Keszthelyi,[b] and Richard Greenberg [a]

[a] *Department of Planetary Sciences, University of Arizona, Tucson, AZ 85721, USA*
[b] *US Geological Survey, 2255 N. Gemini Dr., Flagstaff, AZ 86001, USA*

Received 9 April 2003; revised 16 January 2004

Abstract

Sets of ridges of uncertain origin are seen in twenty-nine high-resolution Galileo images, which sample seven locales on Io. These ridges are on the order of a few kilometers in length with a spacing of about a kilometer. Within each locale, the ridges have a consistent orientation, but the orientations vary from place to place. We investigate whether these ridges could be a result of tidal flexing of Io by comparing their orientations with the peak tidal stress orientations at the same locations. We find that ridges grouped near the equator are aligned either north–south or east–west, as are the predicted principal stress orientations there. It is not clear why particular groups run north–south and others east–west. The one set of ridges observed far from the equator (52° S) has an oblique azimuth, as do the tidal stresses at those latitudes. Therefore, all observed ridges have similar orientations to the tidal stress in their region. This correlation is consistent with the hypothesis that tidal flexing of Io plays an important role in ridge formation.

Keywords: Io; Tides, solid body; Tectonics; Surfaces, satellite

1. Introduction

High-resolution Galileo images of Jupiter's moon Io reveal unexplained ridges on otherwise flat terrain. Although some sites of ridge formation on Io can be attributed to down-slope motion of loose material (Turtle et al., 2001; Moore et al., 2001), these particular ridges do not appear to have formed that way because the plains on which they occur are relatively level (although the slope is admittedly poorly constrained). Figure 1 shows small images of the ridges to scale. For comparison, an example of ridges which are likely to be a result of downslope motion of material on a mountain is shown in Fig. 2 (Turtle et al., 2001).

Each set of ridges under consideration has been examined for nearby volcanic or tectonic features that could control ridge formation; none were observed. Ridge azimuths (measured clockwise from north to the long axis of the ridges) are not systematically oriented with respect to nearby volcanic features. For example, the ridges in Fig. 3 are oriented consistently at 010° on all sides of Chaac Patera, irrespective of the orientation of the patera wall. Also, the ridges do not appear to be tectonically controlled by any nearby mountains or faults. Furthermore, the ridges are probably not a result of buckling of the lithosphere itself since their wavelength is much shorter (0.2–4.0 km) than a reasonable crustal thickness (13–100 km, Jaeger et al. (2003)).

These ridges are morphologically similar to dunes on Earth and Mars. However, Earth and Mars have atmospheric pressures (1×10^5 and 600 Pa, respectively) which are great enough to allow particle transport and hence dune formation. Io's atmosphere has a pressure of $\sim 10^{-5}$ Pa (Kieffer et al., 2000)—much too low to produce dunes such as the ridges we observe. In order to show that dune-like particle transport is unreasonable for Io, we estimate a threshold friction speed for Io. The threshold friction speed is the minimum wind speed necessary to transport a particle, a parameter used when studying dune formation. Greeley and Iversen (1985) have considered threshold friction speeds required for particle transport on Venus, Earth, and Mars. Unfortunately, the semi-empirical equations they present were developed experimentally by wind tunnel testing and are not valid for pressures as low as on Io. Therefore, instead of calculating an exact answer for the threshold friction speed on Io, we perform a rough extrapolation. For Venus, Earth, and Mars,

* Corresponding author.
E-mail address: gwenbart@lpl.arizona.edu (G.D. Bart).

0019-1035/$ – see front matter
doi:10.1016/j.icarus.2004.01.003

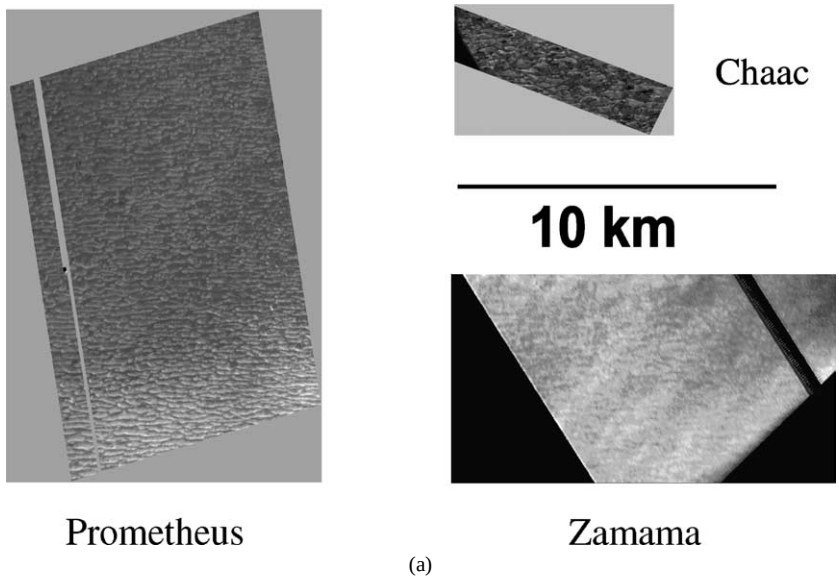

(a)

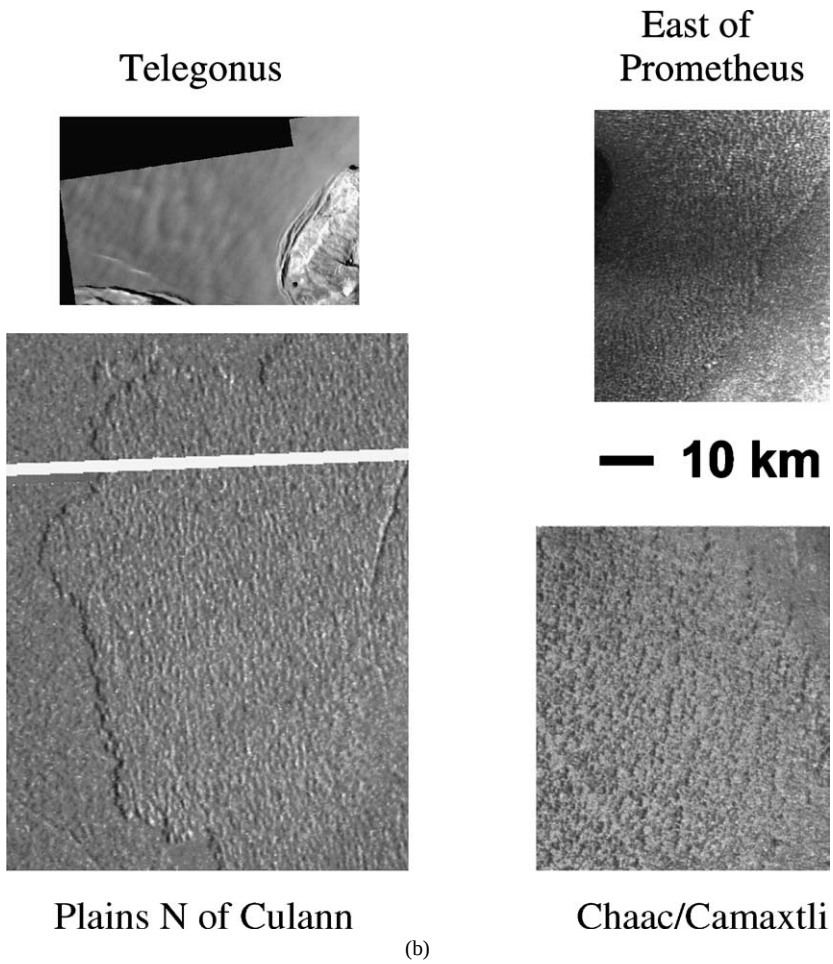

(b)

Fig. 1. Examples of ridge plains to scale. North is up. Name indicates a nearby feature on Io.

Greeley and Iversen (1985) find threshold friction speeds of 2, 20, and 200 cm s^{-1}, respectively. The density ratios (particle density to atmospheric density) they use are 41 for Venus, 2160 for Earth, and 240,000 for Mars. In these cases, the threshold friction speed increases by one order of magnitude as the density ratio increases by two orders of magnitude. Io's density ratio is 5×10^{12} for a 3 g cm^{-3} particle density. Following the same rough trend as seen for Venus, Earth, and Mars, we find the threshold friction speed on Io to be about 20 km s^{-1}. This value is two orders of magnitude greater

Fig. 2. I27 image of ridged surface of Hi'iaka Mons. These ridges are presumed to have formed as a result of down-slope motion, and look similar to the plains ridges we are considering. Orientation of ridges parallel to topographic and tectonic features is indicated by the black arrows. North is up.

than the wind speeds on Io, which have been calculated to be $< 320\ \mathrm{m\,s^{-1}}$ (Ingersoll et al., 1985). Thus, while this is a very rough estimate of the threshold friction speed, it is sufficient to show that Io's winds cannot transport particles to form dunes.

As an alternative, we consider whether tidal stress may have played a role in the formation of these ridges. Io's tides are extraordinarily large because of Io's proximity to Jupiter and its orbital eccentricity, which is forced by its resonance with Europa and Ganymede. As a result, Io's tidal bulge varies significantly in magnitude and direction, driving heat dissipation (Peale et al., 1979). The observed geologic activity is one noticeable result of the tidal heating. Volcanism modifies surface features on time-scales of months and years (Phillips, 2000; Geissler et al., 2004) and may indirectly drive mountain uplift (Schenk and Bulmer, 1998; Turtle et al., 2001; Jaeger et al., 2003).

Another result of Io's high eccentricity and resultant tidal flexing is that its surface goes through a cycle of expansion and contraction (and corresponding tensile and compressive stress) over the course of each orbital period (42.4584 hours). This cycle has the potential to create observable effects depending on the surface composition and structure. No previous study has found evidence for surface deformation caused directly by tidal stress on Io.

There is only one place in the Solar System where there is compelling evidence that surface features are shaped by tidal stress: Europa (Greenberg and Geissler, 2002). The case of Europa, though, is quite different from Io because Europa has an icy lithosphere. Thus, tidal stress can

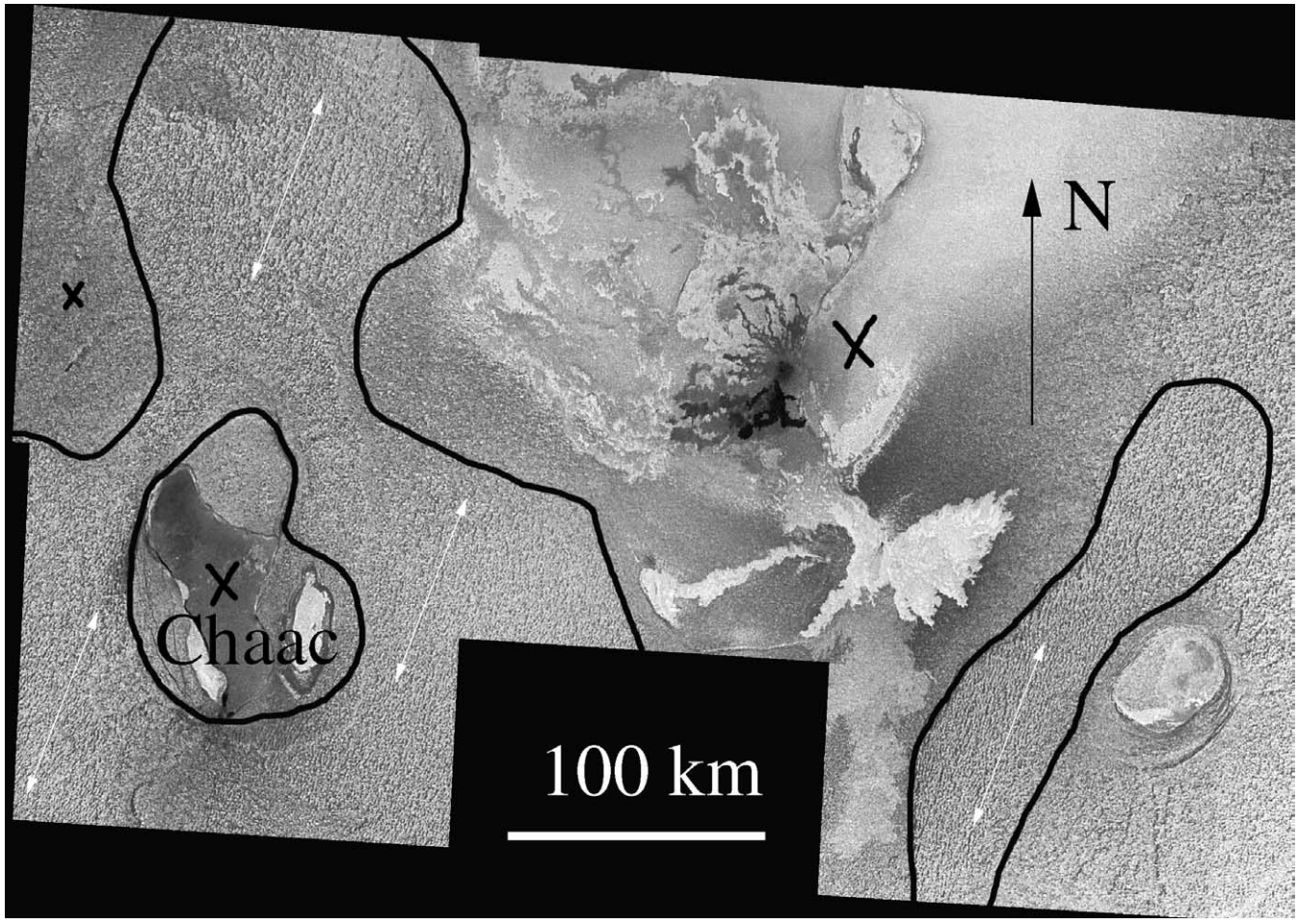

Fig. 3. I27 mosaic (185 m pixel^{-1}) over the Chaac–Camaxtli region with ridges at 12° N, 135° W. Regions with ridges are outlined; white arrows indicate ridge orientation; X's indicate areas without ridges.

result in observable surface features there. For example, when the tension rises high enough on Europa, a crack can fracture the brittle crust and propagate perpendicular to the tensile stress (Lucchitta and Soderblom, 1982; Helfenstein and Parmentier, 1985). Cycloids are one example of cracking being controlled by tidal stress on Europa. Their arcs and cusps have been modeled to have formed in response to changes in tidal stress on Europa over the course of an orbit (Hoppa et al., 2001). Another way tides may affect surface features on Europa is by the repeated opening and closing of cracks. The diurnal tidal cycle could play a part in building the double ridges at the crack location over time (Greenberg et al., 1998).

Surface features similar to Europa's cycloids and double ridges are not seen on Io, which is not surprising since the tidal stresses there are unlikely to be comparable to the tectonic stresses. Furthermore, the ridges seem to form in a mechanically weak volatile surface layer of variable thickness deposited by volcanic plumes (Moore et al., 2001; Keszthelyi et al., 2004). It appears plausible that tidal flexing of the underlying lithosphere has worked this weak surface layer into rolling dune-like ridges. We test that possibility by comparing the orientations of the ridges with the orientations of the peak tidal stresses at their locations. We discuss specific mechanisms by which tides might form these ridges only after showing that there is reason to examine such processes.

2. Observations

Each imaged set of ridges covers at least several square kilometers. The ridges in each locale are oriented in a single direction that is not obviously controlled by nearby geologic features. For example, the ridges in Fig. 3 maintain a constant azimuth of 010° all the way around Chaac Patera. The ridges are parallel to the edge of the patera on the east and west sides and perpendicular to its margin in the north and south. However, at higher resolution, smaller ridges are evident with an azimuth of 088° (Fig. 4). These ridges are truncated by the rim of the patera, clearly indicating that the local topography and volcanic and tectonic features are not governing their orientations. The same situation is seen near Telegonus Mensae (Fig. 5); the ridges are parallel to the eastern scarp but are perpendicular to the southern scarp. If their orientation were being controlled by the scarps we would

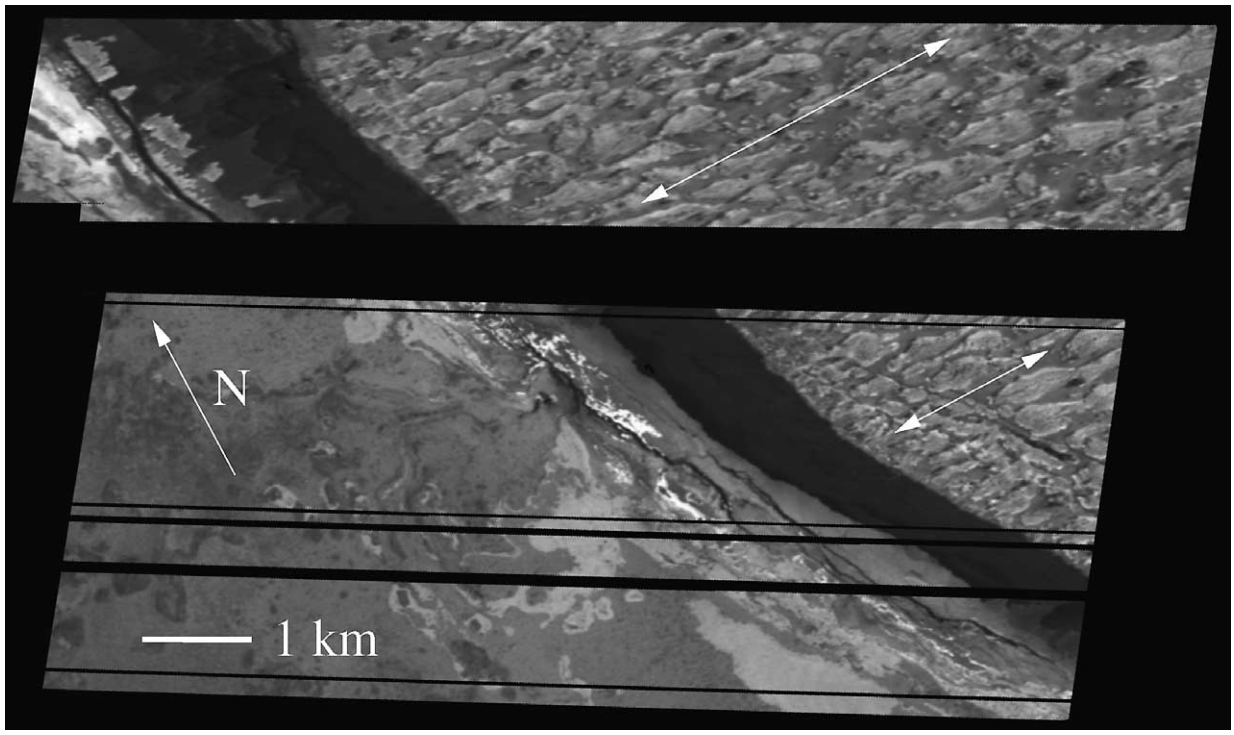

Fig. 4. I27 observations (7 m pixel^{-1}) of Chaac Patera with ridges at 12° N, 157° W oriented east–west, as indicated by the white arrows.

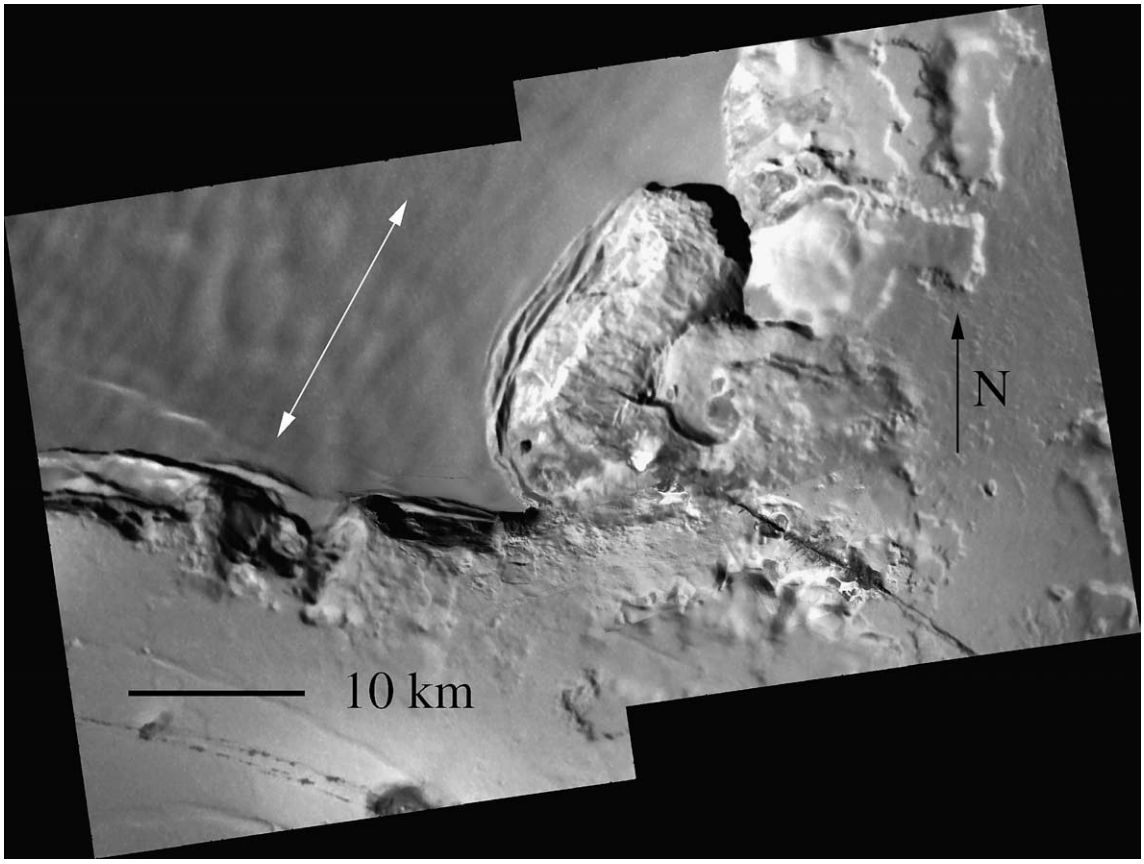

Fig. 5. I27 observation (41 m pixel^{-1}) of Telegonus Mensae with ridges at 52° S, 117° W. The ridges (on the northwest plateau) have an orientation ∼ 030° from north, as indicated by the white arrows.

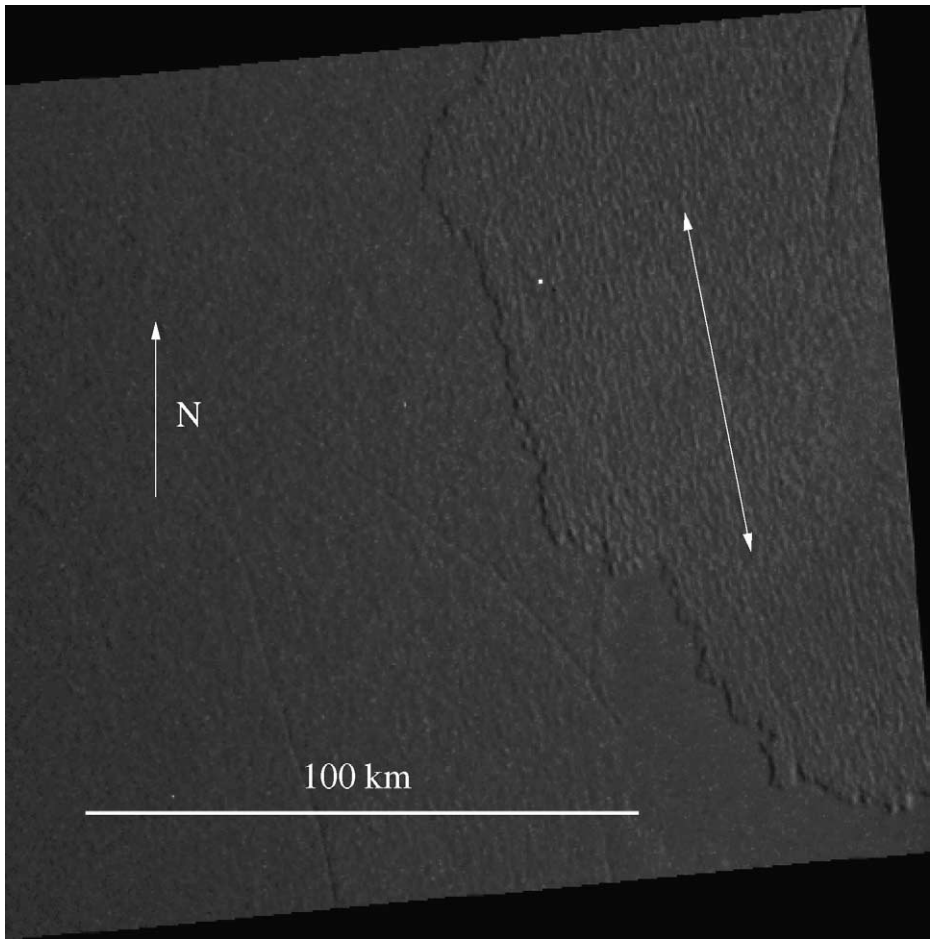

Fig. 6. I32 observation (328 m pixel^{-1}) of plains north of Culann Patera with ridges at 4° S, 166° W. The ridges on the mesa in the eastern portion of the picture trend north–south (as indicated by the white arrows), following neither the edges of the mesa nor the fracture cutting through it.

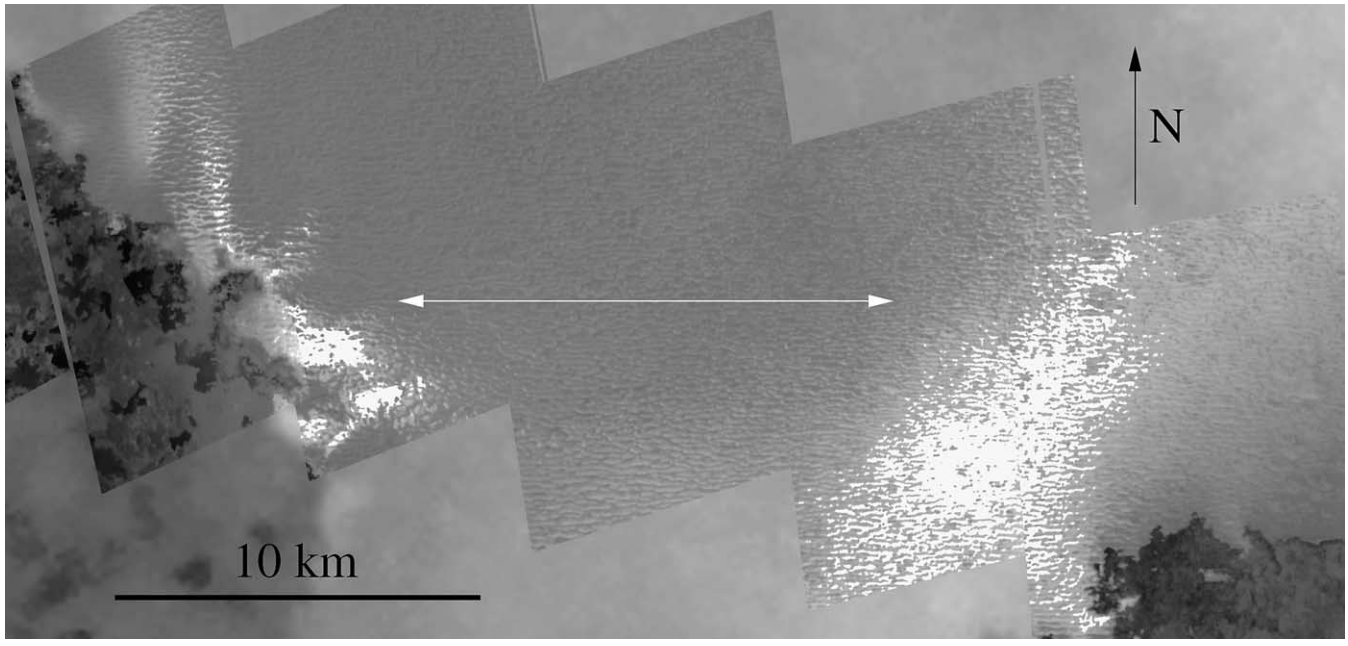

Fig. 7. I27 observation (12 m pixel^{-1}) of part of the Prometheus flow field with ridges at 1° S, 154° W. White arrows indicate the east–west ridge trend.

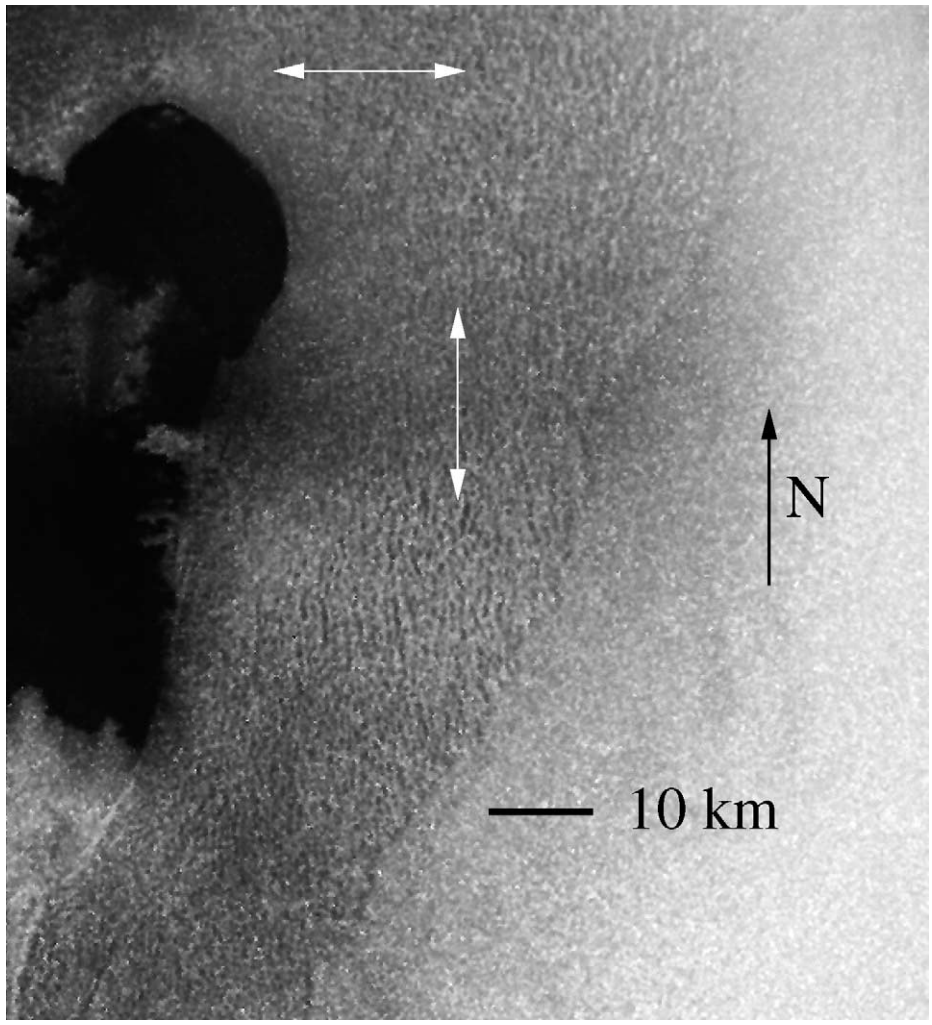

Fig. 8. I27 observation (172 m pixel^{-1}) of Prometheus vent and flows with ridges at 1° S, 151° W. This region appears to have ridges oriented both east–west (near the top of the image, just east of the patera edge) and north–south (a bit farther east and south). White arrows mark their approximate locations. These two sets appear to overlap near the east of the east–west ridges and the north of the north–south ridges.

Table 1
Ridge locations and characteristics

Latitude (°)	Longitude (° W)	Azimuth (°)[a]	Ridge length (km)	Ridge wavelength (km)
12	135	010	6.7 ± 1.7	3.9 ± 0.8
12	157	088	0.8 ± 0.2	0.2 ± 0.1
−52	117	030	5.5 ± 2.2	2.6 ± 0.7
−4	166	170	4.2 ± 1.4	2.2 ± 0.5
−1	154	090	0.6 ± 0.2	0.2 ± 0.1
−1	151	090 and 170	3.1 ± 0.7	0.8 ± 0.2
18	174	090	1.5 ± 0.8	0.2 ± 0.04

[a] Measured clockwise from north to the long axis of ridges, with uncertainty of ±5°.

expect the ridges to be oriented similarly to both. North of Culann Patera (Fig. 6), the ridges also ignore scarps on the relatively featureless plains of Io, and fail to follow the orientation of the tectonic fractures by which they are cross-cut.

The ridge orientation also is independent of nearby lava flows. Figures 7 and 8 show the ridges surrounding the Prometheus flow field. While the ridge orientations include examples with north–south and east–west azimuths, they are not affected by the convoluted margins of the lava flow field. Instead, it appears that the lava is forced to skirt between the ridges. As a final example, the ridges in Fig. 9 near the Zamama flow field also ignore the convoluted flow margins. The consistent orientation of the ridges can be made out despite the image artifacts caused by radiation damage to the camera.

Ridge azimuths were determined by direct measurement of observed ridge orientations and confirmed by two-dimensional Fourier analysis of the images. Fourier trans-

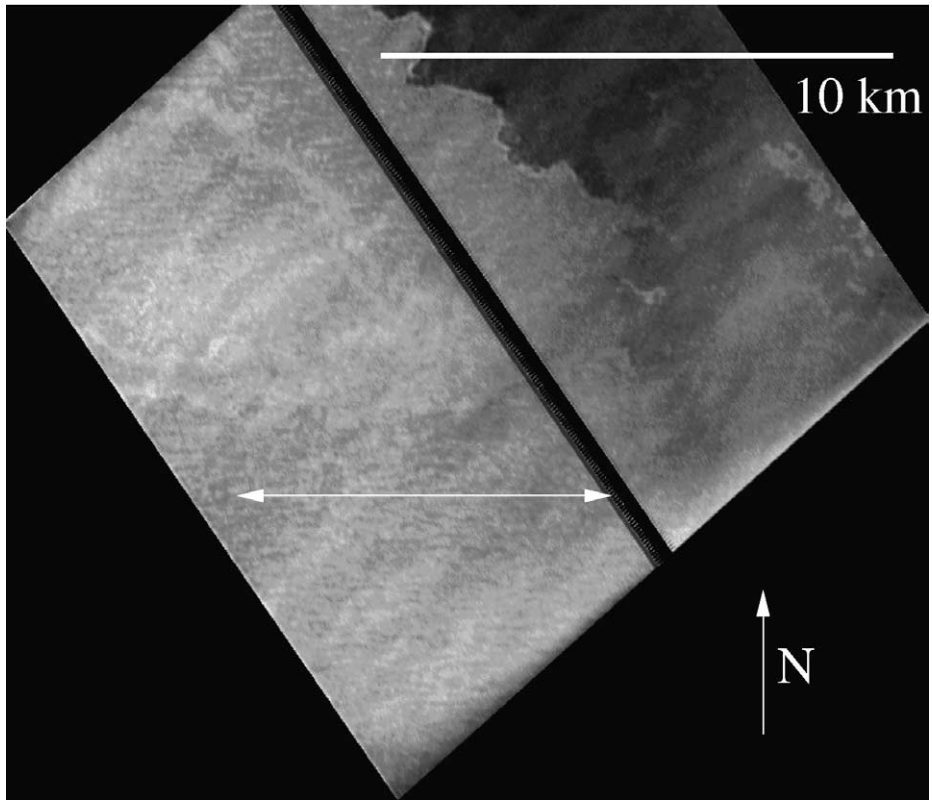

Fig. 9. I24 observation (19 m pixel^{-1}) of Zamama flow field with ridges at 18° N, 174° W. The east–west trend (as indicated by the white arrows) can be observed despite image artifacts due to radiation damage to the camera. The ridges here appear similar to those near Prometheus.

forms (FFTs) are shown for all areas (Fig. 10). The elongation in the frequency domain runs perpendicular to the ridges, confirming the ridge trends. The first FFT shown (Fig. 10a) of the Camaxtli/Chaac region shows a weak directional preference suggesting that in this region the terrain may be better described as hummocky rather than ridged. In contrast, Figs. 10b–10e have stronger signals indicating regular ridges with a clear orientation. Figure 10f shows the Fourier transform of the ridges at Zamama, but this transform is not useful because the I24 data has image artifacts that interfere with Fourier analyses.

Table 1 records characteristics of the observed ridges: their locations, azimuths (measured clockwise from north to their long axis, with uncertainty of ±5°), lengths, and wavelengths (distance between peaks as measured perpendicular to the long axis). Ridge lengths are on the order of a few kilometers (0.5–7.0 km) and ridge spacing is typically ∼ 1 km. Table 2 lists each of the 29 images showing ridges and gives the central latitude and longitude, the incidence angle, the resolution, the area of the image, and the percent of the image in which ridges are seen. The images which show ridges have resolutions $\leqslant 300$ m pixel^{-1}.

The remaining 76 high-resolution ($\leqslant 300$ m pixel^{-1}) Galileo images of Io have solar incidence angles $\geqslant 20°$, which is the solar incidence angle for several of the images that show ridges. Thus ridges should have been visible in these images had they been there. Images with and without ridges are not necessarily isolated from each other; there are cases where images showing ridges occur near several others with no ridges. Adequate images sample the broad region from −50° to 50° latitude and from 45° to 170° W longitude, but generally avoid the plains where ridges are most common. The observed ridges are concentrated near 0° N, 150° W, with only one imaged example near 50° S.

All the image locations are shown graphically in Fig. 11, which plots three things:

(1) the locations and orientations of the ridges in the seven regions where plains ridges are seen,
(2) the locations of Galileo images with resolutions $\leqslant 300$ m pixel^{-1} in which no plains ridges are seen, and
(3) the diurnal stress field at one eighth orbit past apocenter, which will be discussed in Section 3.

Note that in most cases the symbols indicating images are much larger than the image itself, such that the overlap of symbols usually does not indicate that the images overlap. In the field of ridges at longitude 152° W, east of Prometheus (Fig. 8), there appear to be two sets of ridges overprinted on each other, one of which is nearly perpendicular to the other. Thus, in this case Table 1 and Fig. 11 show two ridge azimuths, 090° and 170°, at this location.

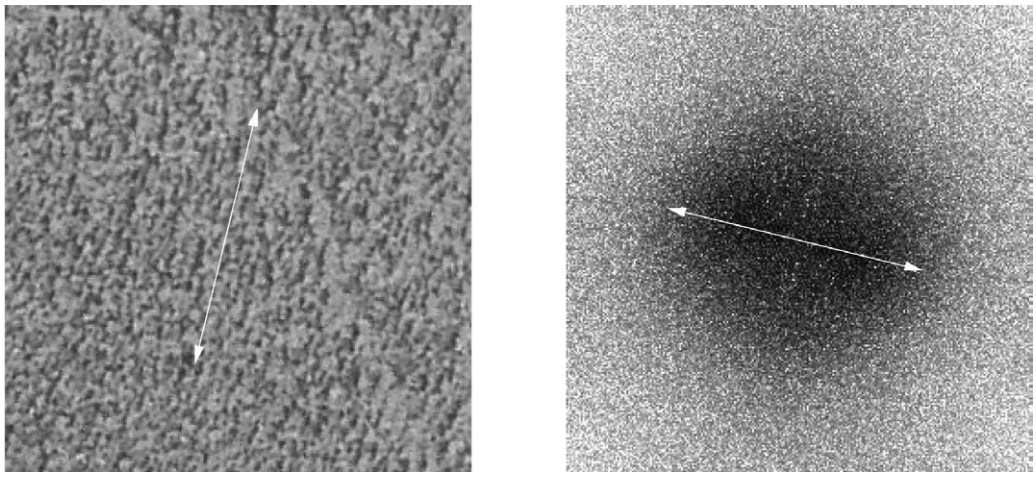

(a)

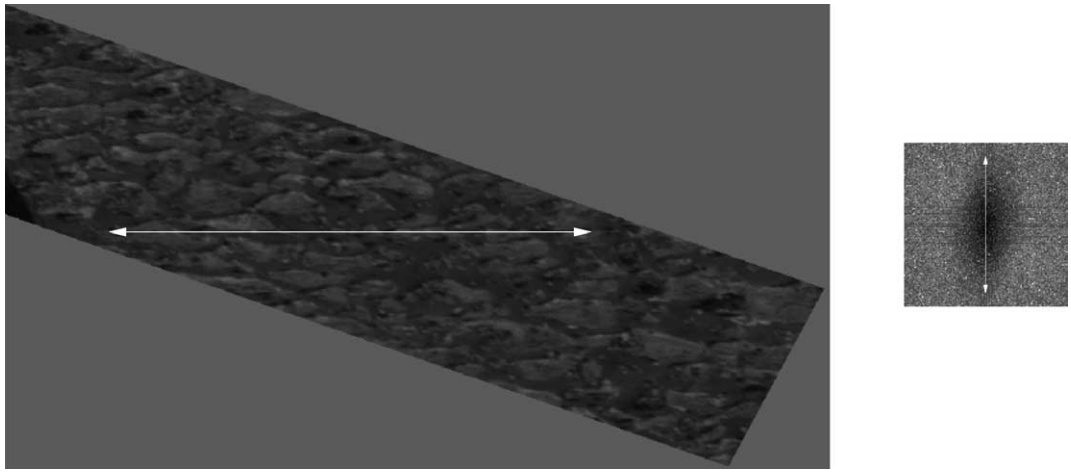

(b)

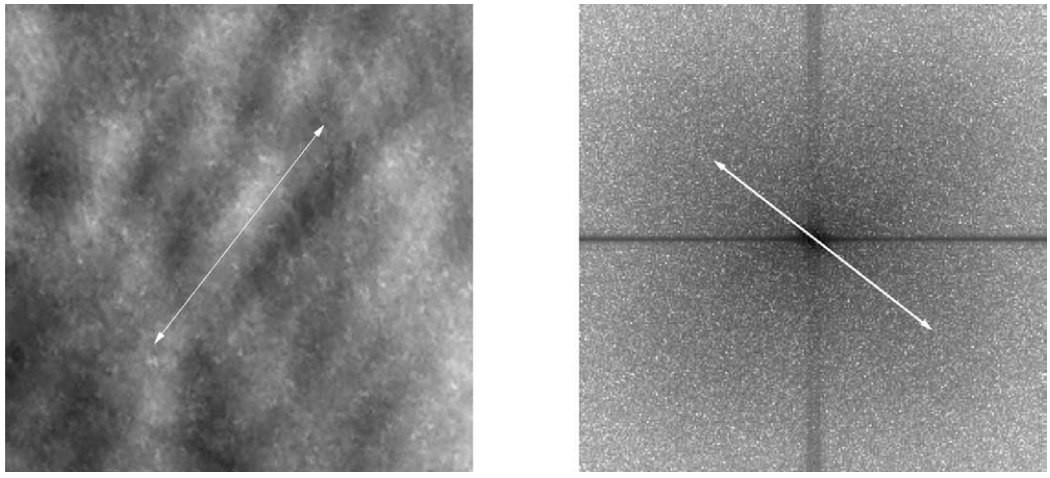

(c)

Fig. 10. Fourier analysis of ridge plains; a polar plot of frequency vs. orientation such that distance from center of plot is frequency. (Left) Sample of ridge plains. (Right) Fourier transform of the scene on the left. The elongation in the frequency domain runs perpendicular to the ridges, confirming the ridge trend at this location. (a) 12° N, 135° W near Camaxtli Patera. (b) 12° N, 157° W near Chaac Patera. (c) 52° S, 117° W near Telegonus. The dark oval on the FFT is admittedly small and hard to see, but it is clearly present upon close examination. (d) 4° S, 166° W north of Culann Patera. (e) 1° S, 154° W near Prometheus. (f) 18° N, 174° W near Zamama. Artifacts from the radiation damage inhibit the usefulness of this FFT.

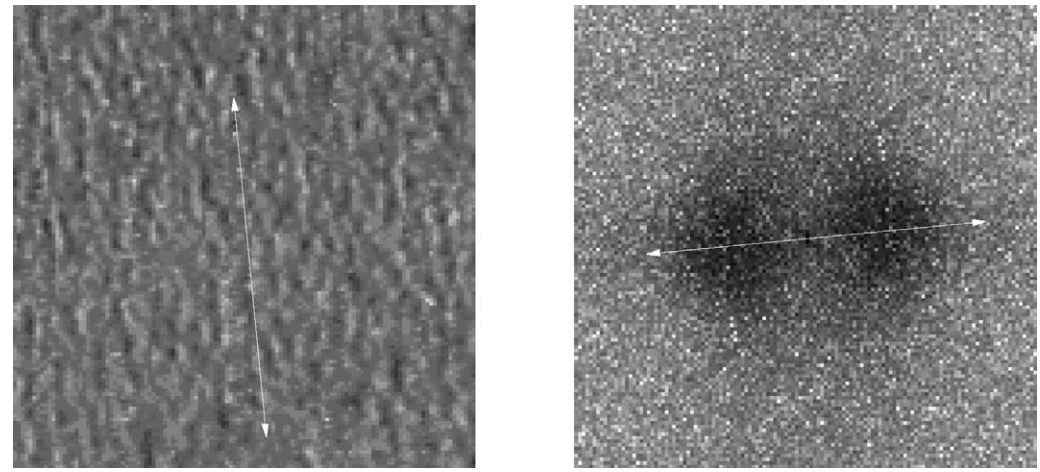

(d)

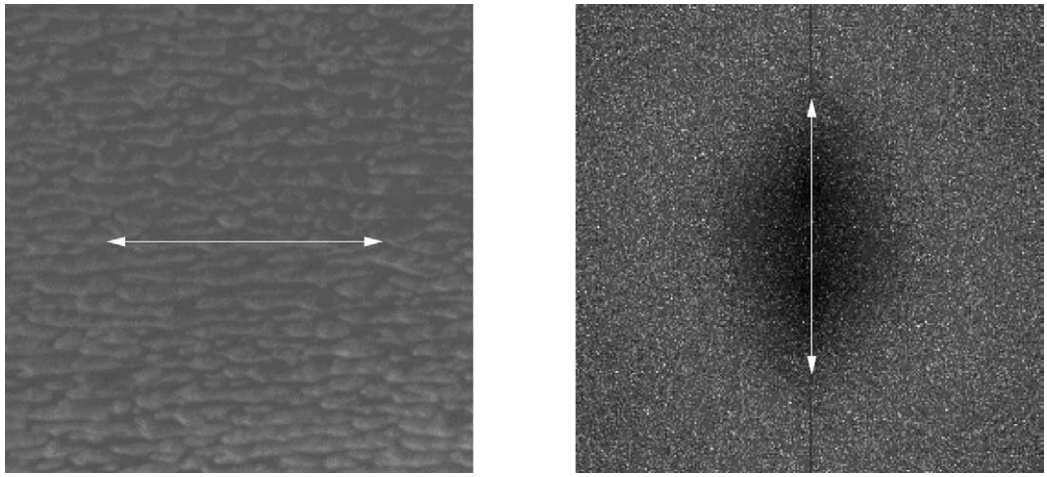

(e)

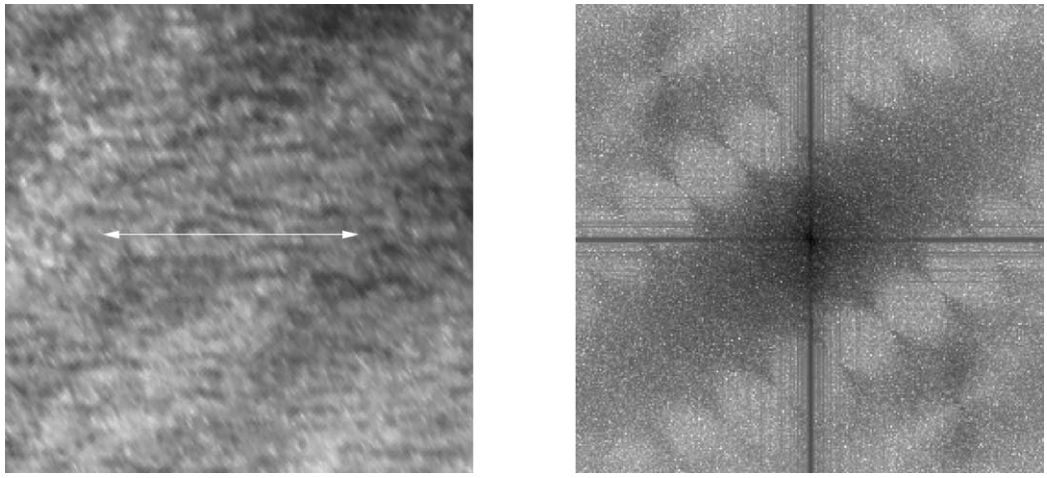

(f)

Fig. 10. Continued.

3. Modeling of tidal stresses

Because of the eccentricity of Io's orbit, the magnitude and direction of the tidal bulge vary throughout an orbit. This deformation causes stress in the lithosphere. We have calculated the magnitude and direction of tidal stresses on Io from the deformation of Io relative to its average figure. The tidal deformation is well known (Jeffreys, 1961) and the magnitude and orientation of the stresses in an elongated or flattened shell were derived by Vening-Meinesz

Table 2
Images showing ridge plains, grouped by region

Galileo SSI image #	Lat (°)	Lon (°)	Incidence angle (°)	Resolution (m pixel^{-1})	Area of image (km^2)	% of image with ridges
e.g., Fig. 3						
0539936400	15	158	21.11	184	30000	100
0539936413	9	154	18.64	184	30000	75
0539936439	11	152	13.94	185	24000	40
0539936452	15	148	13.74	185	24000	25
0539936478	15	143	11.91	186	24000	25
0539936500	11	142	7.68	186	23000	50
0539936526	10	138	7.77	187	23000	30
0539936465	8	144	10.09	185	20000	40
0539936513	12	135	11.86	186	20000	30
e.g., Fig. 4						
0539932065	12.65	157.28	24.64	7	20	80
0539932078	12.47	157.29	24.53	7	40	25
e.g., Fig. 5						
0625594901	−51.99	116.26	62.79	41	1000	12
0625594914	−52.34	117.76	63.69	42	1000	50
e.g., Fig. 6						
0625601253	−8	166	78.81	328	80000	25
0625601266	−1	168	80.83	329	80000	5
e.g., Fig. 7						
0539932265	−1.57	155.15	20.92	11	70	3
0539932278	−1.51	154.96	20.70	11	80	20
0539932300	−1.48	154.75	20.47	11	80	50
0539932313	−1.48	154.53	20.23	12	40	100
0539932326	−1.26	154.48	19.99	12	100	100
0539932340	−1.31	154.23	19.73	13	120	100
0539932353	−1.41	153.97	19.48	14	130	65
0539932365	−1.54	153.70	19.23	14	140	30
e.g., Fig. 8						
0539936113	−1.8	151	11.94	171	20000	12
0539936140	−1.8	151	11.87	172	20000	12
0539936165	−1.8	151	11.86	173	20000	12
e.g., Fig. 9						
0520793656	18.06	174.18	19.49	19	200	80
0520793660	18.00	173.63	19.12	19	200	80
0520793663	17.96	173.22	18.84	19	200	50

(1947); see also Melosh (1977). We follow the method for calculating stresses and cracking on Europa used by Greenberg et al. (1998), except that the following parameters have been changed to fit Io: eccentricity = 0.0041 (Greenberg, 1982), orbital period = 42.4584 hours (Greenberg, 1982), Poisson's ratio = 0.25 (Turcotte and Schubert, 1982), shear modulus = 4.0×10^{10} Pa (Turcotte and Schubert, 1982), and radius = 1821 km. Despite the change of parameters, the stress patterns are qualitatively similar to those on Europa (Hoppa, 1998; Greenberg et al., 1998, 2003).

The first case we consider is that of diurnal stress only. Figure 11, which illustrates diurnal stresses at one eighth orbit past apocenter, gives an example of this case. This example is typical of the diurnal stress fields throughout the orbit (see Hoppa, 1998; Greenberg et al., 2003), and demonstrates patterns that hold regardless of the position in Io's orbit:

(a) principal stresses near the equator tend to be oriented north–south and east–west, with the orientations varying as the latitude increases; and
(b) stresses at high latitudes are generally oriented at more oblique angles.

At any given location on Io's surface, the magnitude and direction of tidal stresses continually change with a 42 hour (1 orbit) periodicity.

In order to illustrate how the stress field changes throughout an orbit, Fig. 12 shows the magnitude and direction of both tensile and compressive stress at six different locations

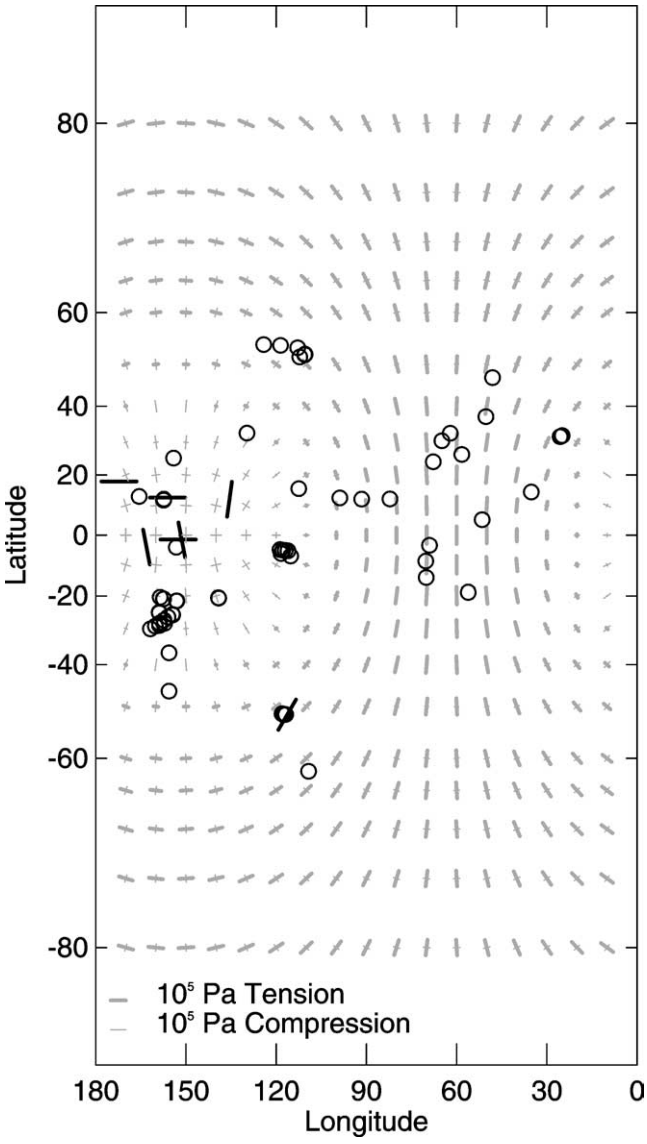

Fig. 11. The locations of ridge plains are each marked with a black line, indicating the azimuth of the observed ridges (Table 1). The center of the line represents the location of the field of ridges. Note that the field of ridges at 1° S, 151° W (Table 1) has two azimuths, both are shown at that location on this map. Also, the ridges at 1° S, 154° W run east–west near the same location, and cannot be distinguished at this scale. The locations of high-resolution images which do not show ridge plains are marked with open circles. The background stress field, in gray, is for diurnal stress at a time one eighth orbit after apocenter. It is shown for the leading hemisphere; the stress field for the trailing hemisphere is identical. The principal stress axes are plotted in gray, with tension indicated by a thick line and compression with a thin line. The length of the line is proportional to the magnitude of the stress. This figure illustrates that stresses near the equator run north–south and east–west, whereas stresses at high latitudes are oriented at more oblique angles. These characteristics of the stress field hold throughout the orbit and are shared by the observed ridge orientations.

every half-hour over the course of one orbit. It can be seen that the stresses near the equator are predominantly oriented north–south and east–west throughout the orbit; however, they do not remain isotropic (Figs. 12a–12d). As the location moves farther from the equator, the stresses vary more from their north–south and east–west orientation. The stresses in Fig. 12e oscillate noticeably about the north–south and east–west orientation. At the ridge location farthest from the equator (Fig. 12f), the stresses vary widely in both character and orientation from those at the other locations. Of the principle stresses at this location, one is tensile while the other is compressive. The orientations of these stresses match the ridge orientation best at pericenter and apocenter.

4. Discussion

The azimuths of observed ridges near the equator are aligned within 10° of either north–south or east–west; theoretical principal stress orientations are similarly oriented roughly north–south and east–west there (Fig. 11). The one set of ridges far from the equator (50° S) has the same oblique azimuth as do theoretical stress orientations at that latitude. The similar orientations of ridges and tidal stresses at each of the seven regions where ridged plains are observed suggests that tidal stresses may have played a role in ridge formation.

However, there are some other issues to consider. For example, although the principal stresses near the equator run both north–south and east–west, it is unclear what would cause ridges to form preferentially in one direction rather than the other, since the principal stresses have similar magnitudes in both directions. An additional factor that can be considered is possible non-synchronous rotation of Io. Non-synchronous rotation is plausible because net tidal torques may be zero at a rotation rate slightly different from synchronous (Greenberg and Weidenschilling, 1984). Non-synchronous rotation would induce an extra stress in Io's lithosphere because as the sub-jovian point rotates from west to east, the tidal bulge will still face Jupiter. Eventually the lithosphere will relax into its new average figure, relieving the stress. Thus the only stress that remains at any given time is from the last degree or so of non-synchronous rotation, depending on the time-scales of non-synchronous rotation and relaxation. We plot diurnal stress at apocenter plus stress accumulated by re-orientation due to possible non-synchronous rotation (Fig. 13). This case shows similar trends to the diurnal case:

(a) principal stresses near the equator are oriented north–south and east–west, with the orientations varying as the latitude increases; and
(b) stresses at high latitudes are generally oriented at more oblique angles.

Thus, potential non-synchronous rotation of Io should not change our conclusion.

Subsequent to formation of a feature, non-synchronous rotation can play yet another role; it can displace already formed features to longitudes east of their present location.

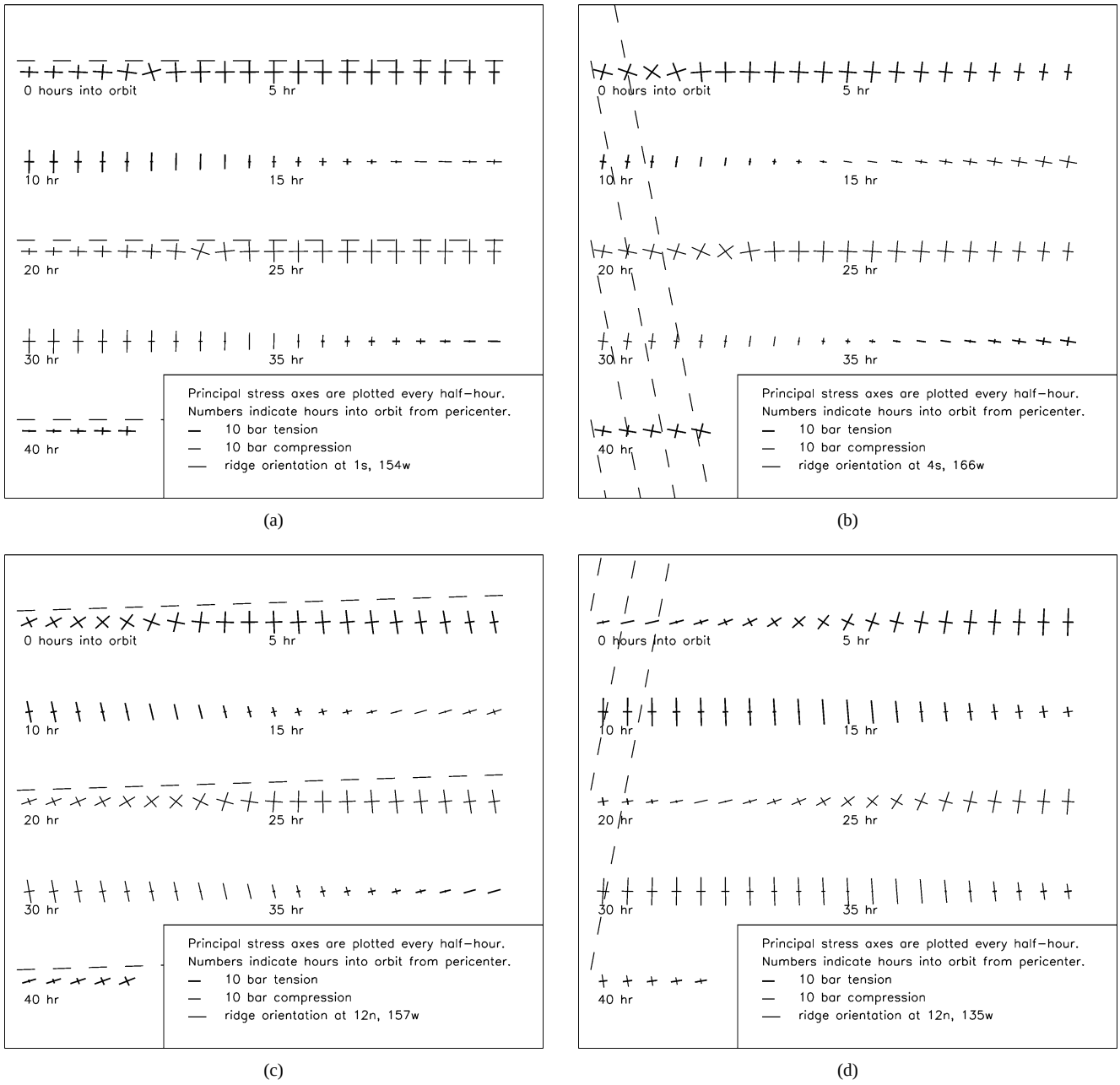

Fig. 12. Illustration of the stresses every half hour through Io's orbit starting at pericenter (0 hours). Read the diagram from left to right to see the sequence of principle stresses in this region. The length of the line indicates the magnitude of the stress, with bold lines for tension and thin lines for compression. The dashed line indicates the ridges trend at that location. (a) 1° S, 154° W near Prometheus. (b) 4° S, 166° W north of Culann Patera. (c) 12° N, 157° W near Chaac Patera. (d) 12° N, 135° W near Camaxtli Patera. (e) 18° N, 174° W near Zamama. (f) 52° S, 117° W near Telegonus.

For this purpose, we can treat the feature just like a flag stuck in the ground where the feature is located. (Of course, if the feature is not static on long time scales, that would need to be considered as well.) Even with such displacement, latitudes still remain constant, so features now near the equator likely formed near the equator, and the ridges near 50° S likely formed at that latitude. Therefore this effect of non-synchronous rotation will not change our conclusion either.

How might we determine whether the ridges have been moved significantly from the longitude where they formed? Milazzo et al. (2001) constrained Io's non-synchronous rotation period to be greater than 1400 years. We have calculated that ridges 100 m high would be covered in less than 10,000 years at the global average volcanic resurfacing rate of $\sim$1 cm year^{-1} (Johnson et al., 1979; Phillips et al., 2000). Thus, unless the period is much shorter than 10,000 years we must be seeing the ridges near the longitude where they formed. Unfortunately, we do not currently have a method by which we can determine whether the period for non-synchronous rotation is greater or less than 10,000 years.

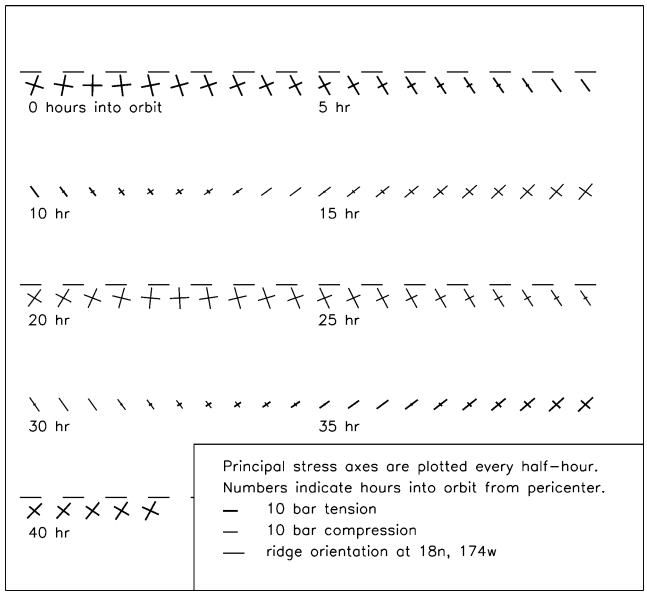

(e)

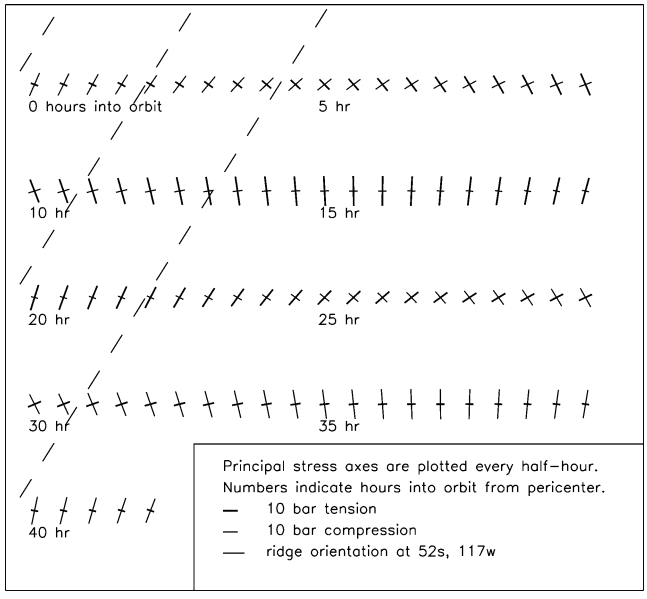

(f)

Fig. 12. Continued.

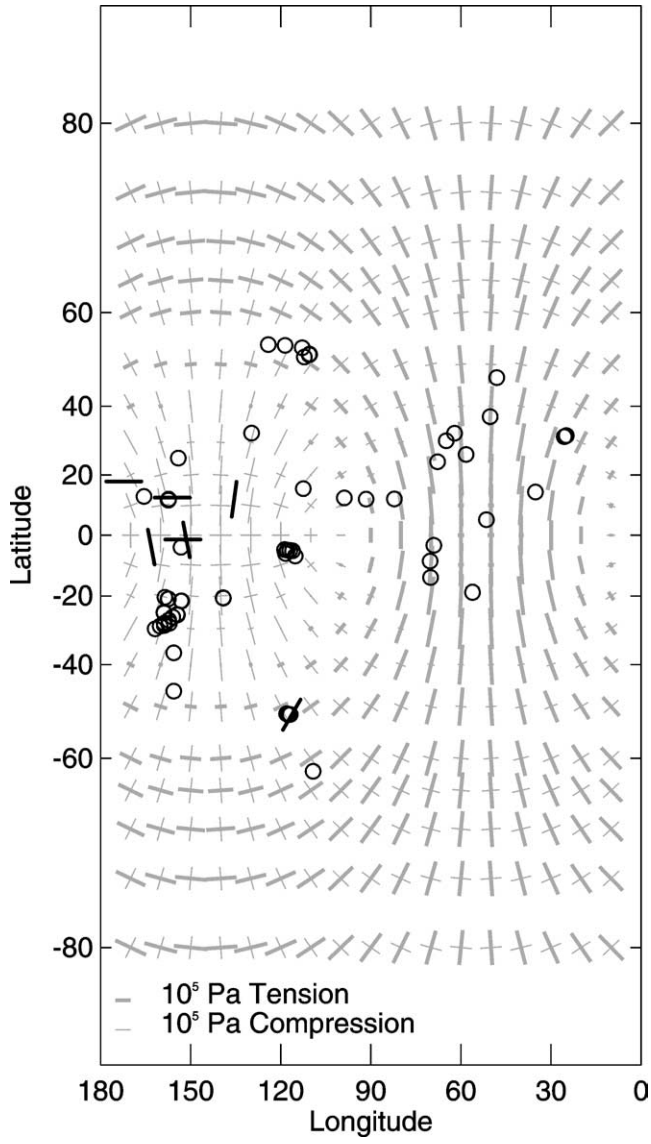

Fig. 13. Similar to Fig. 11 except that here the stress field corresponds to one degree of non-synchronous rotation added to diurnal stress at apocenter. This second example illustrates that theoretical stresses near the equator consistently run north–south and east–west, whereas stresses at high latitudes are oriented at more oblique angles. These orientations are shared by the observed ridge orientations.

There are only 105 high-resolution ($\leqslant 300$ m pixel^{-1}) images of Io from Galileo. Twenty-nine of these images show ridges, and are listed in Table 2. The 76 additional high-resolution ($\leqslant 300$ m pixel^{-1}) images, whose locations are shown in Fig. 11, do not exhibit ridges. Thus about 28% of the available high-resolution images show ridges. The ridges we are considering are located in plains that looked flat and uninteresting in low-resolution coverage. The high-resolution images were targeted at locations known to be of geologic interest: paterae, erupting plumes, mountains, and active lava flows; the plains were only imaged incidentally at these resolutions. In fact, the observed ridges are seen in images targeted at other features: Camaxtli Patera, Chaac Patera, Telegonus Mensae, Tohil Mons, Prometheus, and Zamama. Thus areas which were likely to show ridge plains were systematically excluded in planning high resolution imaging. That 28% of the images do show ridges indicates that these features are indeed quite common on Io.

The patchy presence of ridges built by tidal flexing could also be simply a reflection of the availability of appropriate materials and surface conditions for building and preserving ridges. The regions with abundant observable ridges are particularly rich in volatiles, dominated by SO_2. We speculate that the presence of a blanket of volatiles may be essential for ridge formation.

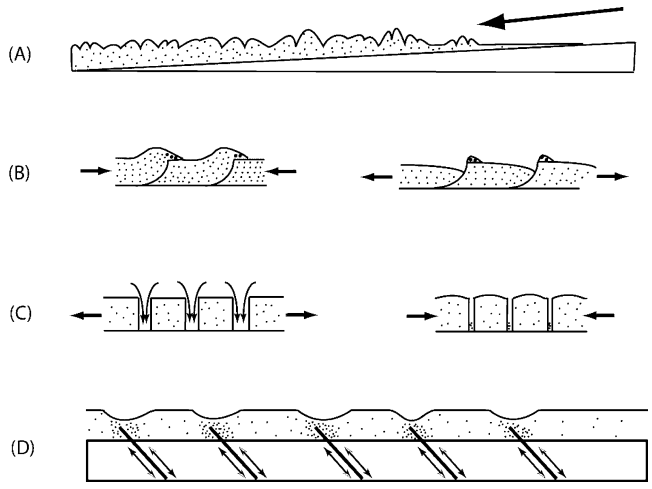

Fig. 14. Schematic cross-sections of several different ridge-formation mechanisms that could be driven by tidal deformation. (A) Tides may allow creep along very shallow slopes, leading to compressional folds. (B) Small amounts of material may be deposited at higher elevation during each compressional cycle of the tides. Over time, this material might build into ridges. (C) Small amounts of material may fall into tensional cracks opened during the extensional cycle of the tides. This material would keep the crack from fully closing during the compressional cycle. Over time, this could produce ridges separated by debris laden depressions. (D) Repeated motion along faults could collapse pore space in a volatile-rich layer, producing elongated depressions. An analogous process is seen on the ocean floor (Davies et al., 1999). Further research is needed to determine which (if any) of these mechanisms is responsible for the Ionian ridges.

Figure 14 shows some possible mechanisms by which tides might form ridges in a volatile-rich surface layer. The most straightforward is that tides could aid gradual creep of material on very shallow slopes. This idea is analogous to the explanation for ridges on mountains (Moore et al., 2001; Turtle et al., 2001). However, it is difficult to imagine that such downslope creep would not be affected by topographic scarps. The presence of scarps highly oblique to the ridges suggests that this may not be the primary mechanism forming ridges in the plains. Furthermore, the ridge orientation would be primarily dependent on the slope direction rather than on the orientation of the tidal stresses.

Repeated motion along discrete fault planes could also produce ridges. As long as each tidal cycle leads to some local small net accumulation (or removal) of material, ridges (or troughs) should form. This process would share some similarity to the proposed double ridge formation process on Europa (Greenberg et al., 1998). Two key differences from Europa are that

(1) new material is not brought into the crust from below, and
(2) the fractures are in a relatively thin layer, leading to much shorter ridge lengths than on Europa.

A final mechanism we consider plausible is a variant on a model for forming kilometer scale hummocks on the sea floor. These form when sediments are compacted by motion on small faults (Davies et al., 1999). On Io, repeated motion along discrete faults due to the tides could compact the mantle of SO_2-rich snow and/or frost.

In some regions the ridges run parallel to the orientation of the maximum tidal stress. Based on the models we are considering, we would expect that the ridges would be perpendicular to the maximum tidal stress. We do not currently have a mechanism to explain the parallel orientations; future work to investigate a model for ridge formation will need to consider this fact.

5. Conclusions

The orientations of the ridges in the plains are consistent with formation from tidal flexing of Io by Jupiter. The orientations of theoretical principal tidal stresses are north–south and east–west near the equator, as are the azimuths of the ridges observed near the equator. Furthermore, the single set of ridges far from the equator (50° S) has an oblique azimuth, as do the stresses in that region. This correlation holds even when stress from non-synchronous rotation is included in addition to diurnal stress. Furthermore, non-synchronous rotation of Io might have moved the ridges from the longitudes at which they were formed, widening the range of possible stress states under which the ridges may have formed. The correlation between ridge azimuth and tidal stress orientation is provocative and provides motivation for future consideration of how and why this correlation exists.

The plains ridges are observed in close proximity to areas which do not exhibit ridges, indicating that tidal stresses alone are not sufficient for ridge formation. It appears that a substantial volatile rich deposit is one of the requirements for ridges. Since high-resolution imaging was targeted at features such as paterae, plumes, and mountains, the flat plains where ridges might occur were not imaged as frequently, and therefore these features may be more common than currently observed. We present some plausible processes by which such a mantle might be modified by tidal stresses to form ridges. However, we need more high-resolution observations and theoretical or experimental modeling of mechanisms for building ridges by tidal flexing to determine the specific ridge formation mechanism acting on Io.

Acknowledgments

We thank Moses Milazzo for help with image processing, Paul Geissler for useful suggestions, and Kandis Lea Jessup for information about Io's atmosphere. We also thank Damon Simonelli and two anonymous reviewers for comments which have significantly improved this paper. This work was supported by NASA grants NAG5-10166 and NAG5-11497 from NASA's Planetary Geology and Geophysics program.

References

Davies, R., Rana, J., Cartwright, J., 1999. Giant hummocks in deep-water marine sediments: evidence for large-scale differential compaction and density inversion during early burial. Geology 27, 907–910.

Geissler, P.E., McEwen, A.S., Phillips, C.B., Keszthelyi, L.P., Spencer, J., 2004. Surface changes on Io during the Galileo mission. Icarus 169, 29–64.

Greeley, R., Iversen, J.D., 1985. Wind as a Geological Process on Earth, Mars, Venus and Titan. Cambridge Univ. Press, Cambridge.

Greenberg, R., 1982. Orbital evolution of the galilean satellites. In: Satellites of Jupiter. Univ. of Arizona Press, Tucson, AZ, pp. 65–92.

Greenberg, R., Geissler, P., 2002. Europa's dynamic icy crust. Meteorit. Planet. Sci. 37, 1685–1710.

Greenberg, R., Weidenschilling, S.J., 1984. How fast do galilean satellites spin? Icarus 58, 186–196.

Greenberg, R., Geissler, P., Hoppa, G., Tufts, B.R., Durda, D.D., Pappalardo, R., Head, J.W., Greeley, R., Sullivan, R., Carr, M.H., 1998. Tectonic processes on Europa: tidal stresses, mechanical response, and visible features. Icarus 135, 64–78.

Greenberg, R., Hoppa, G.V., Bart, G.D., Hurford, T.A., 2003. Tidal stress patterns on Europa's crust. Celest. Mech. Dynam. Astron. 87, 171–188.

Helfenstein, P., Parmentier, E.M., 1985. Patterns of fracture and tidal stresses due to nonsynchronous rotation—implications for fracturing on Europa. Icarus 61, 175–184.

Hoppa, G.V., 1998. Europa: effects of rotation and tides on tectonic processes. PhD thesis. University of Arizona, Tucson.

Hoppa, G.V., Randall Tufts, B., Greenberg, R., Hurford, T.A., O'Brien, D.P., Geissler, P.E., 2001. Europa's rate of rotation derived from the tectonic sequence in the Astypalaea region. Icarus 153, 208–213.

Ingersoll, A.P., Summers, M.E., Schlipf, S.G., 1985. Supersonic meteorology of Io: sublimation-driven flow of SO_2. Icarus 64, 375–390.

Jaeger, W.L., Turtle, E.P., Keszthelyi, L.P., Radebaugh, J., McEwen, A.S., Pappalardo, R.T., 2003. Orogenic tectonism on Io. J. Geophys. Res. Planets 108 (E8), 5093. doi:10.1029/2002JE001946.

Jeffreys, H., 1961. The effect of tidal friction on eccentricity and inclination. Mon. Not. R. Astron. Soc. 122, 339–343.

Johnson, T.V., Cook, A.F., Sagan, C., Soderblom, L.A., 1979. Volcanic resurfacing rates and implications for volatiles on Io. Nature 280, 746–750.

Keszthelyi, L., Jaeger, W.L., Turtle, E.P., Milazzo, M., Radebaugh, J., 2004. A post-Galileo view of Io's interior. Icarus 169, 271–286.

Kieffer, S.W., Lopes-Gautier, R., McEwen, A., Smythe, W., Keszthelyi, L., Carlson, R., 2000. Prometheus: Io's wandering plume. Science 288, 1204–1208.

Lucchitta, B.K., Soderblom, L.A., 1982. The geology of Europa. In: Satellites of Jupiter. Univ. of Arizona Press, Tucson, AZ, pp. 521–555.

Melosh, H.J., 1977. Global tectonics of a despun planet. Icarus 31, 221–243.

Milazzo, M.P., Geissler, P.E., Greenberg, R., Keszthelyi, L.P., McEwen, A.S., Radebaugh, J., Turtle, E.P., 2001. Non-synchronous rotation of Io? In: Jupiter: Planet, Satellites, and Magnetosphere Conference. Abstract 75–76.

Moore, J.M., Sullivan, R.J., Chuang, F.C., Head, J.W., McEwen, A.S., Milazzo, M.P., Nixon, B.E., Pappalardo, R.T., Schenk, P.M., Turtle, E.P., 2001. Landform degradation and slope processes on Io: the Galileo view. J. Geophys. Res. 106, 33223–33240.

Peale, S.J., Cassen, P., Reynolds, R.T., 1979. Melting of Io by tidal dissipation. Science 203, 892–894.

Phillips, C., 2000. Voyager and Galileo SSI views of volcanic resurfacing of Io and the search for geologic activity on Europa. PhD thesis. University of Arizona, Tucson.

Phillips, C.B., McEwen, A.S., Keszthelyi, L.P., Geissler, P.E., Simonelli, D.P., Milazzo, M., the Galileo Imaging Team, 2000. Volcanic resurfacing rates and styles on Io. Bull. Am. Astron. Soc. 32, 1046. Abstract 29.05.

Schenk, P.M., Bulmer, M.H., 1998. Origin of mountains on Io by thrust faulting and large-scale mass movements. Science 279, 1514–1517.

Turcotte, D.L., Schubert, G., 1982. Geodynamics: Applications of Continuum Physics to Geological Problems. Wiley, New York.

Turtle, E.P., Jaeger, W.L., Keszthelyi, L.P., McEwen, A.S., Milazzo, M., Moore, J., Phillips, C.B., Radebaugh, J., Simonelli, D., Chuang, F., Schuster, P., the Galileo SSI Team, 2001. Mountains on Io: high-resolution Galileo observations, initial interpretations, and formation models. J. Geophys. Res. 106, 33175–33200.

Vening-Meinesz, F.A., 1947. Shear patterns of the Earth's crust. Trans. Amer. Geophys. Union 28, 1–61.